scientific reports

Check for updates

OPEN

Leveraging dynamics informed neural networks for predictive modeling of COVID-19 spread: a hybrid SEIRV-DNNs approach

Cheng Cheng[1], Elayaraja Aruchunan[2] & Muhamad Hifzhudin Noor Aziz[1]✉

A dynamics informed neural networks (DINNs) incorporating the susceptible-exposed-infectious-recovered-vaccinated (SEIRV) model was developed to enhance the understanding of the temporal evolution dynamics of infectious diseases. This work integrates differential equations with deep neural networks to predict time-varying parameters in the SEIRV model. Experimental results based on reported data from China between January 1, and December 1, 2022, demonstrate that the proposed dynamics informed neural networks (DINNs) method can accurately learn the dynamics and predict future states. Our proposed hybrid SEIRV-DNNs model can also be applied to other infectious diseases such as influenza and dengue, with some modifications to the compartments and parameters in the model to accommodate the related control measures. This approach will facilitate improving predictive modeling and optimizing public health intervention strategies.

Keywords COVID-19, Transmission dynamics, Neural networks, DINNs

In the rapidly evolving COVID-19 pandemic, traditional epidemiological models have struggled to account for dynamic factors such as new variants and shifting public health policies[1,2]. The emergence of the novel coronavirus SARS-CoV-2, the causative agent of COVID-19, was initially identified in December 2019 in Wuhan, Hubei province, China[3]. The virus quickly precipitated a global health emergency. Within a month of the first reported case, the virus had manifested in several countries, compelling the World Health Organization (WHO) to declare it a public health emergency of international concern by the end of January 2020[4]. As the virus disseminated globally, its trajectory was punctuated by the emergence of several variants. The Alpha variant (B.1.1.7), first identified in the United Kingdom, marked the beginning of a perilous phase of rapid global spread[5]. Then the Delta variant (B.1.617.2) detected in India became predominant, its heightened transmissibility exacerbating the pandemic's second wave[6]. The relentless evolution of the virus saw further iterations with the Beta (B.1.351) and Gamma (P.1) variants, each contributing to the complex epidemiological landscape. However, the Omicron variant (B.1.1.529), first reported in South Africa in November 2021, underscored the pandemic's unpredictable nature with its multitude of mutations and potential for immune evasion[7]. Over the span of 3 years, these variants have challenged public health interventions, testing the resilience of global health systems and the adaptability of scientific responses[8].

The application of mathematical models in the COVID-19 pandemic has been paramount in dissecting the mechanisms of spread, forecasting epidemiological trends, evaluating the efficacy of control interventions, and optimizing containment strategies. Central to these models are data fitting and parameter estimation, which are foundational yet critical components for understanding and simulating the dynamics of disease transmission[9,10]. Amid the real-world scenario of shifting control policies, vaccination rollouts, and the emergence of new viral variants, the temporality of parameters becomes a significant consideration. Analyzing factors that influence public health behaviours, such as individuals' intentions to receive COVID-19 vaccine boosters, is crucial. Understanding these factors can guide efforts to increase booster vaccination rates, which remains essential for effective pandemic control[11]. Capturing the temporal variability in disease transmissibility is essential to accurately assess the effectiveness of non-pharmaceutical interventions (NPIs) or vaccination campaigns[12]. Traditional mechanism-based models typically predefine specific transmission (or contact) rate functions

[1]Institute of Mathematical Sciences, Faculty of Science, Universiti Malaya, 50603 Kuala Lumpur, Malaysia. [2]Department of Decision Science, Faculty of Business and Economics, Universiti Malaya, 50603 Kuala Lumpur, Malaysia. ✉email: hifz_din@um.edu.my

to simulate a declining trend, alongside another distinct function that captures the increasing trend to track significant events that enhance or mitigate the impact of NPIs or the vaccination timelines[13].

However, to accommodate multiple epidemic trajectories, models require the integration of more specific functions and parameters. The limited information available in datasets and constraints in the speed of response to adverse indicators undoubtedly pose a substantial challenge to data fitting and parameter estimation, simultaneously amplifying the issue of parameter unidentifiability. This remains a critical issue that the field currently faces[14]. The complexity of modeling is further exacerbated by the need to continuously adapt and fine-tune models to reflect the evolving landscape of the pandemic. As new data emerge and our understanding of the virus deepens, iterative model refinements are necessary. This iterative process includes incorporating the impact of behavioural changes, government-imposed restrictions, and biological factors such as immunity waning and reinfection rates[15]. The real-time recalibration of models is vital to maintain their relevance and predictive accuracy as the pandemic progresses. Moreover, researchers have turned to advanced computational techniques and machine learning algorithms to enhance the robustness of parameter estimation. These methodologies allow for the exploration of vast parameter spaces and can identify patterns that might not be immediately evident through traditional means[16].

Deep neural networks (DNNs) have permeated a wide array of disciplines, revolutionizing approaches in data mining, natural language processing, pattern recognition, medical diagnostics, fault diagnosis, and genomics[17–21]. Within infectious disease modeling, DNNs present distinct advantages, effectively capturing the complex, nonlinear patterns associated with disease transmission. Neural networks have shown superior accuracy over traditional univariate time series models in forecasting healthcare metrics, such as COVID-19 case numbers and mortality[22]. A study in Pakistan found that artificial neural networks outperformed other time series models in predicting COVID-19 deaths and recoveries, highlighting the accuracy and usefulness of neural network models in healthcare forecasting[23]. A pivotal attribute of DNNs is their universal approximation property, which allows them to approximate the state variables of mechanistic models, such as differential equations, and their time-dependent parameters[24]. The adoption of DNNs in the domain of infectious disease modeling offers a paradigm shift from traditional analysis, providing a robust framework for capturing the complex biological, behavioral, and social factors that drive epidemic spread[25]. This is particularly relevant in the context of COVID-19, where the virus's transmission dynamics are influenced by a myriad of factors including governmental policies, community responses, and the intrinsic properties of the virus itself[26]. Moreover, the integration of DNNs allows for a more nuanced understanding of the temporal evolution of the pandemic, accommodating shifts in virus dynamics due to mutations, and changes in population behavior due to interventions such as lockdowns and mask mandates[27]. Such an approach is invaluable in informing the strategic deployment of resources, timing of intervention measures, and the potential necessity for vaccine deployment and modification in the face of viral evolution[28]. The DINNs model's capacity for real-time learning from data can provide forecasts that are critical for decision-makers, offering insights into the efficacy of current interventions and the necessity for their alteration or continuation[29].

The central research question this study addresses revolves around the application of DINNs in capturing the complexity of infectious disease spread, particularly in the context of the COVID-19 pandemic. We develop a novel DINNs framework that integrates compartmental models with the predictive power of deep learning to estimate time-dependent epidemiological parameters accurately. This is particularly significant in capturing the dynamic nature of COVID-19 spread as it factors in the temporal changes in policy interventions, behavioral adaptations, and viral evolution.

Mini-review of related works

The intersection of traditional infectious disease modeling and machine learning offers a transformative approach to understanding and predicting the spread of diseases. Traditional epidemiological models, such as the Susceptible-Infected-Recovered (SIR) and its derivatives, have provided foundational insights into disease dynamics by segmenting populations based on disease status[30]. These compartmental models, which are grounded in differential equations, have been instrumental in forecasting disease trajectories and assessing the potential impact of public health interventions[31]. However, a significant limitation of SIR and SEIR models is their assumption of static parameters, which makes them ill-suited for capturing real-time changes in transmission dynamics due to evolving factors such as policy interventions, vaccination rollouts, and the emergence of new viral variants[32,33]. These models often fail to adapt to the dynamic nature of pandemics, thereby reducing their predictive accuracy and applicability in rapidly changing environments.

The advent of machine learning, especially deep learning techniques[18], has markedly improved conventional epidemic models through sophisticated parameter estimation and long-term trend forecasting. Deep neural networks (DNNs) are essential for modelling intricate transmission dynamics, facilitating the estimate of time-dependent parameters that are difficult to capture using traditional methods[34]. Utilising their layered design, DNNs proficiently capture non-linear correlations in extensive datasets[35], hence enhancing the calibration and forecasting precision of epidemiological models[36]. Furthermore, ensemble approaches that amalgamate many machine learning models have exhibited enhanced robustness and accuracy in predicting infectious disease outbreaks[37]. The integration of mechanistic models with deep neural networks (DNNs) encompasses parameter inference, whereby sophisticated methods like Bayesian optimisation enable a thorough investigation of parameter spaces, hence improving model calibration to empirical data[38]. This hybrid modelling technique enhances the prediction capability of conventional models and delivers profound insights into epidemic dynamics, therefore furnishing more dependable decision-support tools for public health managers[39].

Deep neural networks (DNNs) has significantly advanced infectious disease modeling by enabling direct data-driven approaches that capture complex biological processes relying on predefined equations[40]. Recent studies have demonstrated the efficacy of recurrent neural networks (RNNs) and long short-term memory

(LSTM) networks in modeling the temporal dynamics of COVID-19, effectively predicting its spread by learning from sequential case data[41]. DNNs excel in identifying intricate, non-linear relationships within large datasets, thereby enhancing the precision and predictive capabilities of epidemiological analyses[42]. Unlike traditional compartmental models such as the susceptible-exposed-infected-recovered (SEIR) framework, which assume homogeneous population mixing and often overlook complex social behaviors and networks[43], DNNs can account for heterogeneities and the stochastic nature of real-world interactions that drive disease transmission[44]. Additionally, DNNs facilitate parameter estimation in complex disease dynamics, providing estimates for transmission and recovery rates, as well as the impacts of interventions[45]. Real-time prediction models continuously update with new data, enabling the assessment of public health measures as they are implemented[46]. Their ability to integrate diverse data sources-including clinical data, mobility patterns, and social media trends-allows for a comprehensive analysis of factors influencing disease spread[47]. The flexibility of DNN architectures permits their adaptation to various modeling tasks, from forecasting case numbers to evaluating non-pharmaceutical interventions[48].

This study proposes a novel approach that leverages the power of machine learning, specifically deep neural networks (DNNs), to unravel the intricate epidemiological dynamics often obscured in the study of COVID-19 spread. The proposed method, termed as SEIRV-dynamics-informed neural networks, incorporates prior knowledge from the SEIRV model into the loss functions of DNNs as a physical regularizer. This innovative approach extends beyond the conventional SIR model by including additional compartments for exposed individuals (E) and vaccinated populations (V), enabling a more comprehensive representation of the complex dynamics at play. To assess the efficacy of the SEIRV-dynamics-informed neural networks, the method is first tested against synthetic data generated from the SEIRV model under various scenarios. Subsequently, the approach is validated using real-world COVID-19 data reported from China between January 1, 2022, and December 1, 2022, sourced from the COVID-19 Data Repository maintained by Johns Hopkins University. The incorporation of the SEIRV model's ordinary differential equations (ODEs) into the DNN's learning process allows for an efficient and accurate approximation of the underlying complex dynamics.

Methodology

Dynamic model

The SEIRV model is an epidemiological model that extends the classic SEIR model by incorporating vaccination dynamics to account for the mitigating effects of vaccine deployment in a population. Each compartment in the model represents a different stage of how the disease spreads through a population. The susceptible (S) group includes people who could potentially catch the infection. The exposed (E) group consists of those who have come into contact with the virus but are not yet able to spread it. The infectious (I) group includes those who can transmit the disease to others. The recovered (R) group represents people who have had the infection, recovered, and are now immune. Finally, the vaccinated (V) group includes individuals who have been vaccinated, which lowers their chance of getting infected. The addition of the vaccinated class allows public health officials and researchers to simulate and understand the impact of vaccination strategies on the spread of an infectious disease. Recent research employed the SEIRV model to assess the influence of vaccination on the COVID-19 pandemic[49]. The corresponding differential equations for the SEIRV model are given by Eq. (1):

$$\begin{aligned}
\frac{dS}{dt} &= -\frac{\beta SI}{N} - \varepsilon S, \\
\frac{dE}{dt} &= \frac{\beta SI}{N} + \frac{\alpha \beta VI}{N} - \sigma E, \\
\frac{dI}{dt} &= \sigma E - \gamma I - \mu I, \\
\frac{dR}{dt} &= \gamma I, \\
\frac{dV}{dt} &= \varepsilon S - \frac{\alpha \beta VI}{N}.
\end{aligned} \tag{1}$$

In these equations, N represents the total population and is defined as the sum of all compartmental populations, $N = S + E + I + R + V$. The parameter β denotes the transmission rate of the disease, σ is the rate at which exposed individuals become infectious, γ is the recovery rate, ϵ is the vaccination rate, causing vaccinated individuals to become susceptible again[50].

Figure 1 presents the flowchart of the SEIRV model, illustrating the dynamic interactions among the different compartments: Susceptible (S), Exposed (E), Infectious (I), Recovered (R), and Vaccinated (V). Vaccination (V) serves as a critical mechanism in shaping population dynamics, facilitating the transition of individuals from the Susceptible (S) compartment to the Vaccinated (V) compartment at a rate ϵ. By reducing the number of individuals vulnerable to infection, vaccination significantly curtails the transmission potential of the disease.

DNN architecture

The architecture of deep neural networks (DNNs) is inspired by the biological neural networks that constitute animal brains. A DNN is composed of multiple layers of artificial neurons or nodes, each designed to perform specific transformations on the data. The typical architecture includes an input layer, several hidden layers, and an output layer[17,51]. The performance of DNNs can be attributed to their depth, which allows the networks to

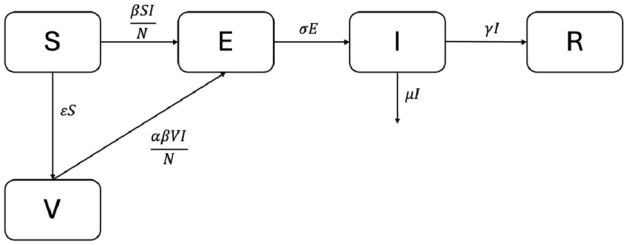

Fig. 1. Flowchart of the SEIRV epidemiological model. This diagram illustrates the core components and dynamic transitions between compartments in the SEIRV model, including susceptible (S), exposed (E), infected (I), recovered (R), and vaccinated (V) populations. Arrows between the compartments represent how individuals transition due to disease transmission, recovery, or vaccination.

learn complex patterns and hierarchies of features. The deeper layers can create abstract representations of the input data, making DNNs highly effective for tasks such as image and speech recognition, natural language processing, and more[52,53]. Combining deep neural networks (DNNs) with the SEIRV epidemiological model can be done to enhance the model's predictive capability. The universal approximation theorem, which states that a feed-forward network with a single hidden layer containing a finite number of neurons can approximate continuous functions on compact subsets of $\mathbb{R}^n$, justifies the use of DNNs for such tasks[54].

In our implementation, we utilize a DNN architecture with five hidden layers. The choice of five layers strikes a balance between model complexity and computational efficiency, providing sufficient depth to capture the nonlinear dynamics of the SEIRV epidemiological model without leading to overfitting. For activation functions, we have chosen the Rectified Linear Unit (ReLU) as the primary activation function in our hidden layers. ReLU is favored due to its computational efficiency and ability to mitigate the vanishing gradient problem, which is prevalent in deeper networks when using activation functions like sigmoid or hyperbolic tangent (tanh). The ReLU function allows for faster convergence during training and helps maintain strong gradients, facilitating effective learning in deep architectures[55]. Additionally, we have incorporated L2 regularization to prevent overfitting by penalizing large weights, thus enhancing the generalization capability of our model. We also included dropout layers, which randomly deactivate a subset of neurons during training, further preventing overfitting and promoting a robust model that generalizes well to new data..

The training of DNNs is typically done through backpropagation, an algorithm that calculates the gradient of the loss function with respect to the network's weights, adjusting them to minimize the loss[18]. For optimizing the parameters of the DNNs, algorithms such as stochastic gradient descent (SGD), Adam, and RMSprop are often used. These optimizers adjust the weights to minimize a loss function, typically a form of mean squared error (MSE) when dealing with continuous output like $\beta(t)$[56].

To apply DNNs to the SEIRV model, one might construct a DNN for the SEIRV Model: This network would aim to simulate the dynamics of the SEIRV model itself, learning from the data how the different compartments interact over time. The network would be trained simultaneously with the same objective: to minimize the difference between the predicted values and the actual data on the spread of the disease.

DINNs model

The coupling strategy and parameter-sharing mechanism in integrating deep neural networks (DNNs) with the SEIRV model involves using the DNNs to numerically solve the system of ordinary differential equations (ODEs). Using one set $S_{NN}(t), E_{NN}(t), I_{NN}(t), R_{NN}(t)$ for the state variables. The DNN for solving the SEIRV model, outputs approximations of the compartments, aiming to solve the ODEs given the current estimates of $v(t)$ from DNN_v. This methodology effectively creates a feedback loop. The networks share parameters through this feedback mechanism, leading to a coherent model that aligns with the underlying disease spread dynamics. Figure 2 illustrates the architecture of the Dynamics Informed Neural Networks (DINNs), which comprises an input layer, fully connected hidden layers with nonlinear activation functions, and an output layer. The network updates the state of neurons across layers via weight matrices w and biases b. Dedicated neural networks are deployed to infer the dynamic parameters, observed states, and unobserved states at each discrete time t_n.

The loss function for the DINNs framework can be designed to comprise two main components: the model loss, which ensures the outputs from the neural network adhere to the SEIRV differential equations, and the data loss, which quantifies the discrepancies between the network outputs and the actual epidemiological data. This dual-component loss function is pivotal for the network to learn both the dynamics of disease transmission and fit the empirical data.

The model loss (L_{model}) ensures that the predictions from the neural networks for the susceptible ($S_{NN}(t)$), exposed ($E_{NN}(t)$), infected ($I_{NN}(t)$), recovered ($R_{NN}(t)$) and vaccinated ($V_{NN}(t)$) adhere to the dynamics described by the SEIRV differential equations. The data loss (L_{data}) could be defined using mean squared error (MSE) for various epidemiological data points such as daily new cases ($C_{new}(t)$), cumulative cases ($C_{cum}(t)$), daily vaccinations ($V_{new}(t)$), and cumulative vaccinations ($V_{cum}(t)$). The total loss function L_{total} is then a weighted sum of these two losses:

$$L_{total} = L_{model} + L_{data} \tag{2}$$

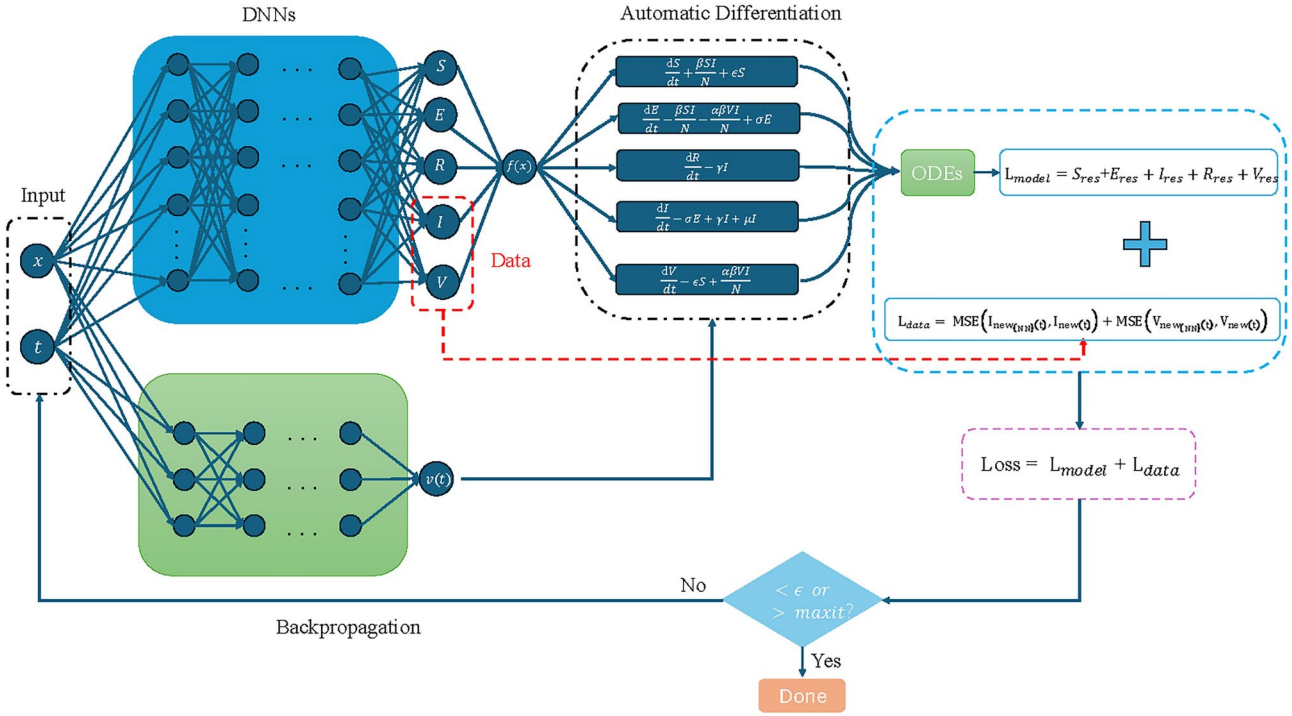

Fig. 2. Schematic diagram of the dynamics informed neural networks. This model is designed for simultaneous data fitting and solution of ordinary differential equations (ODEs) associated with the SEIRV epidemiological framework and incorporates two deep neural networks (DNNs) to optimize the model parameters and solve the ODEs by minimizing the mean squared error (MSE). The training process persists until either a predefined error threshold is achieved or a maximum number of iterations is completed.

As described in the model, the data loss calculation is given by which takes into account both the new cases and the vaccination data.

$$L_{data} = \text{MSE}(I_{new_{NN}}(t), I_{new}(t)) + \text{MSE}(V_{new_{NN}}(t), V_{new}(t)) \tag{3}$$

The model loss (L_{model}) for the SEIRV model in the context of a deep neural network would satisfy the following system of differential equations:

$$\begin{aligned}
\frac{dS_{NN}(t)}{dt} &= -\beta_{NN}(t)\frac{S_{NN}(t)I_{NN}(t)}{N} - \varepsilon_{NN}(t)S_{NN}(t),\\
\frac{dE_{NN}(t)}{dt} &= \beta_{NN}(t)\frac{S_{NN}(t)I_{NN}(t)}{N} + \alpha_{NN}(t)\beta_{NN}(t)\frac{V_{NN}(t)I_{NN}(t)}{N} - \sigma_{NN}(t)E_{NN}(t),\\
\frac{dI_{NN}(t)}{dt} &= \sigma_{NN}(t)E_{NN}(t) - (\gamma_{NN}(t) + \mu_{NN}(t))\, I_{NN}(t),\\
\frac{dR_{NN}(t)}{dt} &= \gamma_{NN}(t)I_{NN}(t),\\
\frac{dV_{NN}(t)}{dt} &= \varepsilon_{NN}(t)S_{NN}(t) - \alpha_{NN}(t)\beta_{NN}(t)\frac{V_{NN}(t)I_{NN}(t)}{N},
\end{aligned} \tag{4}$$

The loss function L could be designed to minimize the error between the observed data and the model predictions over time. Typically, this would be achieved by using the sum of squared errors (SSE) between the observed compartmental values and those predicted by the model:

$$\begin{aligned}
L(\theta) = \sum_{t=1}^{T} \Big[&(S_{\text{obs}}(t) - S_{\text{NN}}(t))^2 + (E_{\text{obs}}(t) - E_{\text{NN}}(t))^2 + (I_{\text{obs}}(t) - I_{\text{NN}}(t))^2 \\
&+ (R_{\text{obs}}(t) - R_{\text{NN}}(t))^2 + (V_{\text{obs}}(t) - V_{\text{NN}}(t))^2 \Big]
\end{aligned} \tag{5}$$

where θ represents the set of all model parameters. $S_{obs}(t), E_{obs}(t), I_{obs}(t), R_{obs}(t), V_{obs}(t)$ are the observed values of the compartments at time t. $S_{NN}(t), E_{NN}(t), I_{NN}(t), R_{NN}(t), V_{NN}(t)$ are the values predicted by the neural network model at time t. T is the total number of time points at which data are available.

Equation (6) is the model loss can be formulated as the sum of the squares of the residuals for these equations:

$$L_{\text{model}} = \sum_t \left(\left(\frac{dS_{\text{NN}}(t)}{dt} + \beta_{\text{NN}}(t) \frac{S_{\text{NN}}(t) I_{\text{NN}}(t)}{N} + \varepsilon_{NN}(t) S_{NN}(t) \right)^2 + \ldots + \left(\frac{dV_{\text{NN}}(t)}{dt} - \varepsilon_{NN}(t) S_{NN}(t) + \alpha_{NN}(t) \beta_{NN}(t) \frac{V_{NN}(t) I_{NN}(t)}{N} \right)^2 \right) \tag{6}$$

where the sum runs over the time steps, and the ellipsis (...) stands for similar terms for the E, I, R, D, and V compartments.

Experiments and results

This section first outlines the process for generating synthetic data using the SEIRV model, followed by the preprocessing of the reported data from China. Subsequently, the architecture and specifics of the physics-informed neural networks developed for these scenarios are detailed. Finally, the efficacy of the proposed DINNs is evaluated using the testing datasets.

Data preparation

We obtained COVID-19 data for China from the Johns Hopkins University Center for Systems Science and Engineering (JHU CSSE)[57]. This dataset includes daily reported cases, daily deaths, cumulative reported cases, and cumulative deaths. Vaccination data were sourced from "Our World in Data", encompassing daily vaccination numbers as well as cumulative vaccination totals[58].

The reliability and cleanliness of reported data are critical for the predictability of compartmental models, especially in terms of parameter estimation. However, due to issues such as misreporting and delays in reporting, the data available is considerably noisy. The data reported from China exhibits significant differences between weekdays and weekends, attributed to a substantial reduction in testing volume during weekends. Consequently, the ability to make valuable estimates from the available reported data is limited. To further process outliers and missing values, we use the interquartile range (IQR) method to identify outliers. Data points below $Q_1 - 1.5 \times IQR$ or above $Q_3 + 1.5 \times IQR$ are considered outliers[59]. To ensure data consistency, outliers and missing data points are processed by averaging the values immediately adjacent to the mean. This method takes into account the information on both sides of the missing value, better balances possible fluctuations, and reduces the deviation during the filling process. Subsequently, to remove dimensionality, we applied min-max normalization to scale the data within the [0,1] range.

$$x_{\text{norm}} = \frac{x - \min(x)}{\max(x) - \min(x)} \tag{7}$$

where x_{norm} is the normalized value, x is the original value, $\min(x)$ is the minimum value in the dataset, and $\max(x)$ is the maximum value in the dataset. Prior to data analysis, we preprocessed the dataset by applying a 7-day moving average window to eliminate the serrated variations due to weekday-weekend cycles in the epidemic reporting. As illustrated in Fig. 3, the reported data from different compartments, post-moving window preprocessing, appear significantly smoother and less noisy compared to the original data.

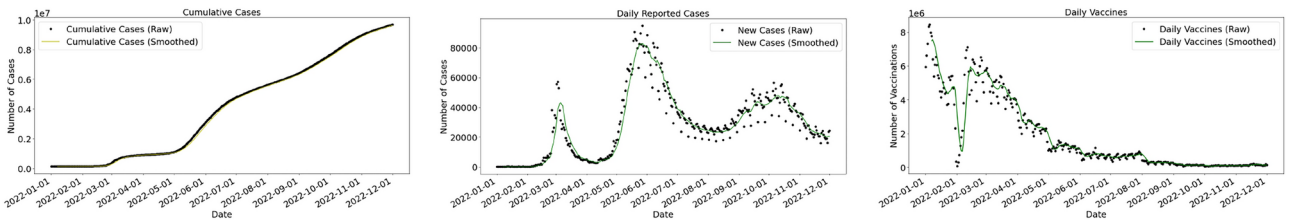

a. Cumulative cases **b.** Daily cases **c.** Daily vaccines

Fig. 3. Comparison of reported data before and after preprocessing. Each subplot corresponds to cumulative cases, daily cases, and daily vaccinations respectively. Black dots represent the raw, unprocessed data, while the green solid line illustrates the data smoothed via a moving window.

Model training and predictions

We implement the dynamics informed neural networks (DINNs) method using the Python programming language and the TensorFlow framework[60]. Each neural network developed in this study consists of 5 layers. The weights and biases of each layer, denoted as W_k and b_k respectively, are structured as follows: $W_1 \in \mathbb{R}^{1\times 35}$, $W_2 \in \mathbb{R}^{35\times 50}$, $W_3 \in \mathbb{R}^{50\times 30}$, $W_4 \in \mathbb{R}^{30\times 30}$, $W_5 \in \mathbb{R}^{30\times 20}$, and $b_1 \in \mathbb{R}^{35}$, $b_2 \in \mathbb{R}^{50}$, $b_3 \in \mathbb{R}^{30}$, $b_4 \in \mathbb{R}^{30}$, $b_5 \in \mathbb{R}^{20}$. Table 1 lists the parameters and their corresponding values used in the epidemiological models.

The neural network architecture employed in our experiments is designed to take a single scalar input, the time t. Each hidden layer of the network is characterized by weight matrices $W_{i,j}$, where i denotes the position of the start node and j indicates the position of the end node. The non-linear activation function applied at each hidden node is the hyperbolic tangent function, defined as 8:

$$\tanh(x) = \frac{e^{x} - e^{-x}}{e^{x} + e^{-x}}. \tag{8}$$

For the output nodes, a sigmoid activation function is utilized to normalize the outputs corresponding to $S(t), E(t), I(t), R(t)$, and $V(t)$. The sigmoid function is given by 9:

$$\sigma(x) = \frac{1}{1 + e^{-x}}. \tag{9}$$

The neural network consists of 5 hidden layers, each containing 50 neurons. The Adam optimization algorithm[56], as implemented in the TensorFlow package, was selected to train the network. The initial learning rate was set to 0.001, with training conducted over 10,000 epochs. To mitigate the risk of overfitting and to enhance the generalization capability of the model, a learning rate decay mechanism was incorporated, reducing the learning rate by 95% every 2000 epochs. The entire training process spans approximately 7 min for 10,000 epochs over all the training data.

By utilizing the model, we can predict future trends of the epidemic. The modeling results can provide reliable feedback for future decision-making by authorities. To evaluate the fitting performance of the proposed DINNs method against observed data from January 1, to December 1, 2022, we visualize the training data in Fig. 4. Figure 4a represents the daily data of new infections, while Fig. 4b shows the daily vaccination data. The DINNs model demonstrates significant accuracy in aligning with the general epidemic pattern and well accommodates the observed data points. The fitted curve effectively represents the three major epidemic peaks throughout this era. Nevertheless, the model exhibits minor discrepancies, which are ascribed to abrupt policy alterations or unexpected changes in population behavior that the model parameters cannot entirely include. Notwithstanding these slight discrepancies, the model effectively encapsulates many waves of infections, illustrating its resilience and flexibility to intricate epidemic patterns. Furthermore, as shown in Fig. 5, the value of the loss function ensures the convergence of the proposed DINNs method for the SEIRV partition model.The loss steadily decreases, indicating successful convergence of the DINNs model. Employing a learning rate decay method to diminish the learning rate by 95% every 2000 epochs alleviates the risk of overfitting and enhancing the model's generalization capability.

We tested the predictive capability of the proposed method by forecasting the outbreak of COVID-19 in China. The compartmental model based on ordinary differential equations (ODEs) requires the determination of initial conditions and model parameters to make predictions. Since the initial conditions can be obtained from the training data and the model parameters have already been calibrated, we can predict the epidemic dynamics by executing the forward process.

Model evaluation performance

Moreover, to quantitatively evaluate the performance of the proposed DINNs method, we employed five evaluation metrics for fair and effective comparison: mean absolute error (MAE), mean squared error (MSE), root mean squared error (RMSE), mean absolute percentage error (MAPE) and R^2. MAE directly interprets the average error in the same units as the data, making it easy to understand typical prediction deviations. MSE and RMSE are sensitive to large errors, highlighting significant deviations between the model and the actual value,

Parameter	Description	Value
α	Rate of transition from exposed to infectious	$1/3$[61]
γ	Recovery rate of infectious individuals	$1/10$[61]
σ	Rate at which exposed individuals become infectious	0.1781[34]
ϵ	Vaccination rate	Fitted
β	Transmission rate	Fitted
$\frac{1}{c}$	Vaccine onset period	14 days[62]
$\frac{1}{\alpha}$	Incubation period	3.4 days[63]

Table 1. Parameters and their values used in the epidemiological and neural network models.

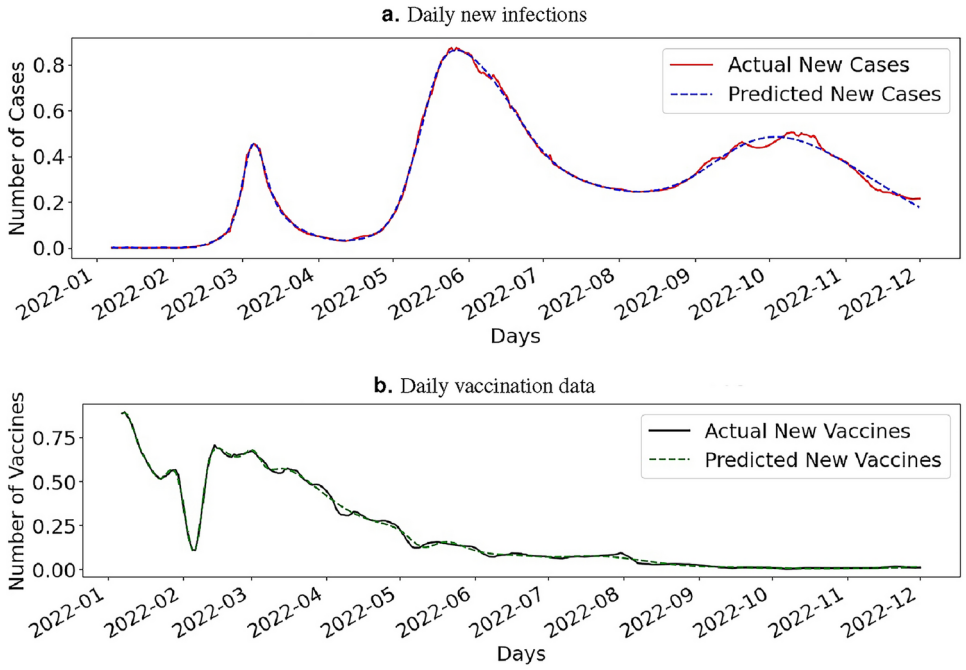

Fig. 4. Fitted curves for (**a**) daily new infections and (**b**) daily vaccination data. The realized depiction displays the actual data, whilst the dotted line illustrates the outcome of the fit.

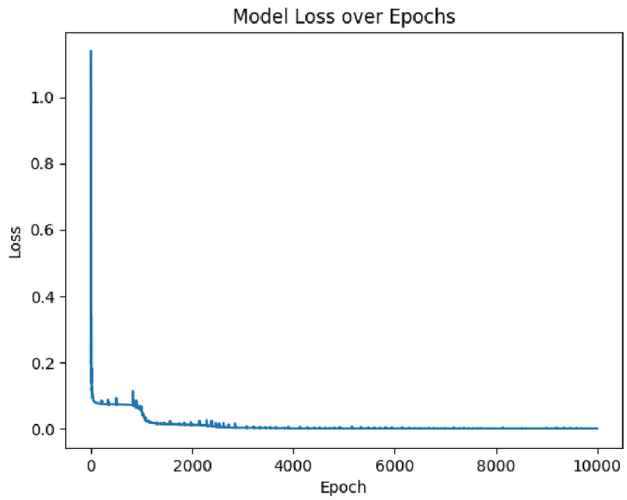

Fig. 5. Loss function during the training process. The figure illustrates the trajectory of the loss value as the DINNs model undergoes training epochs. A steady decline in the loss indicates successful convergence, while stabilization suggests that the model has effectively minimized prediction errors.

which is crucial for identifying potential outbreaks or sudden changes in vaccination rates. MAPE expresses the prediction accuracy as a percentage, which facilitates comparison of the performance of different scales of infection or vaccination data. The R^2 metric assesses the proportion of the variance in the observed data that is explained by the model, providing insight into the overall fit and predictive power. The calculation methods are shown in Eqs. (10), (11), (12), (13), and (14). .

$$\text{MAE} = \frac{1}{n}\sum_{i=1}^{n}|y_i - \hat{y}_i| \tag{10}$$

$$\text{MSE} = \frac{1}{n}\sum_{i=1}^{n}(y_i - \hat{y}_i)^2 \tag{11}$$

Compartment	MAE	MAPE (%)	RMSE	MSE	R^2
S	0.3087	1.50	0.3738	0.1397	0.8389
I	0.0085	0.12	0.0118	0.0001	0.9973
V	0.0084	0.16	0.0129	0.0001	0.9971

Table 2. Metrics for SEIRV compartments.

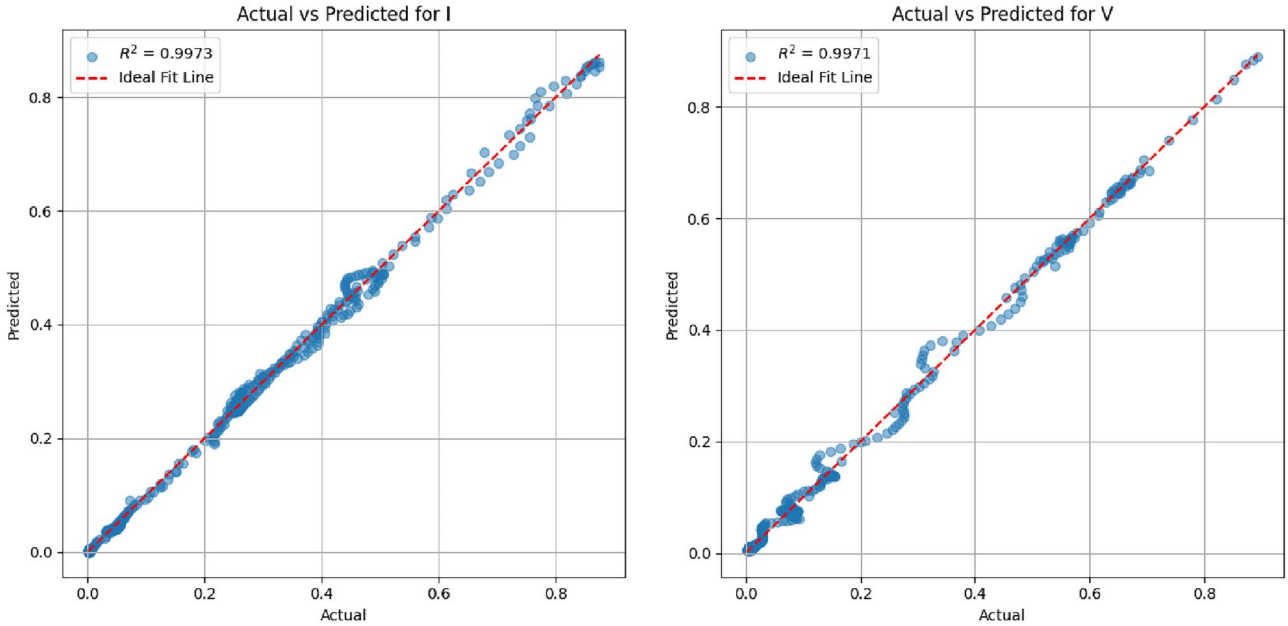

a. Actual vs Predicted for I **b.** Actual vs Predicted for V

Fig. 6. Scatter plots demonstrating the predicted versus actual results for infectious (I) and vaccine (V) compartments. Black dots represent observed values, while the solid red line illustrates the ideal fit line. The R^2 scores highlight the goodness of fit to the observed data.

$$\text{RMSE} = \sqrt{\frac{1}{n}\sum_{i=1}^{n}(y_i - \hat{y}_i)^2} \tag{12}$$

$$\text{MAPE} = \frac{100\%}{n}\sum_{i=1}^{n}\left|\frac{y_i - \hat{y}_i}{y_i}\right| \tag{13}$$

$$R^2 = 1 - \frac{\sum_{i=1}^{n}(y_i - \hat{y}_i)^2}{\sum_{i=1}^{n}(y_i - \bar{y})^2} \tag{14}$$

where y_i and $\hat{y}_i$ represent the actual and predicted values, respectively, and n is the total number of data points. The MAE, MSE, RMSE, MAPE, R^2 and MAPE values are calculated for the predicted daily new cases and daily vaccinations, providing a comprehensive evaluation of the proposed DINNs method's performance.

Experimental results as represented in Table 2 show the highly accurate forecasting capability of the proposed method. The findings indicate that the DINNs model has significant predictive accuracy, particularly in the I and V intervals, characterized by low MAE, MAPE, RMSE, and MSE values, with elevated R^2 scores. The RMSE of 0.0118 and MSE of 0.0001 for the infectious (I) category further underscore the model's precision in representing the dynamics of the infectious population. The RMSE of 0.0129 and MSE of 0.0001 for the vaccine (V) are minimal, underscoring the model's proficiency in reliably forecasting vaccination trends. The elevated error rate in the susceptible (S) can be ascribed to the intrinsic difficulty of modeling susceptible populations, influenced by several factors including behavioral modifications, governmental interventions, and disparate immunity rates. Furthermore, Fig. 6 displays scatter plots that compare the predicted versus actual values for the infectious (I) and vaccinated (V) compartments. The black dots represent observed data points, while the solid red line signifies the ideal fit where predictions perfectly match observations. The high R^2 scores for

Width	Depth		
	5	10	15
30	8.19e−4	4.36e−4	1.06e−3
40	8.86e−4	3.24e−4	3.21e−4
50	3.06e−4	3.44e−4	3.04e−4

Table 3. Final loss values for different model depths and widths.

Metric	DINN	Traditional model
Training time (s)	431.78	0.10
Memory usage (MB)	255.31	107.34
Inference time (s)	0.0021	0.0023

Table 4. Computational Complexity Comparison between DINNs and Traditional SEIRV Parameter Estimation Methods.

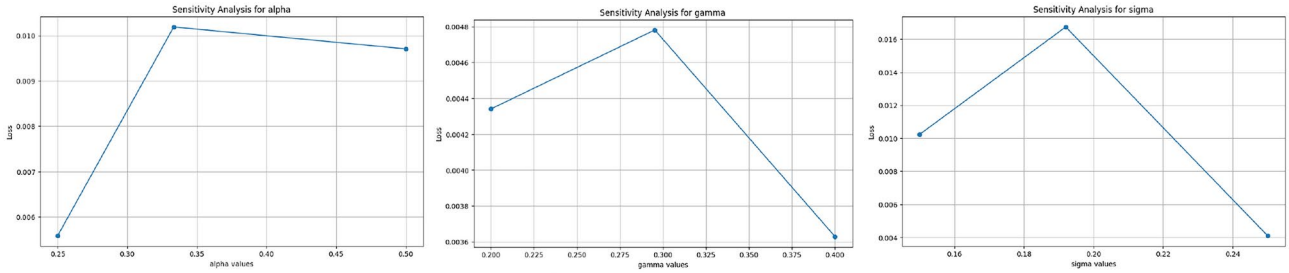

a. α changes effect **b.** γ changes effect **c.** σ changes effect

Fig. 7. Quantitative Sensitivity Analysis of DINNs Model Parameters. Effects of α, γ, and σ Variations on Model Outputs.

both compartments highlight a strong correlation between the model's predictions and the actual data, thereby validating the DINNs model's effectiveness in accurately capturing the complex dynamics of COVID-19 spread and vaccination efforts. These scatter plots demonstrate that the model's predictions are consistently close to the real-world data, affirming its reliability for forecasting infectious disease trends.

Computational complexity

Given the complexity of the DINNs model, we analyzed its computational complexity. During the training phase, the computational complexity of the DINNs model primarily depends on the depth and width of the neural network. We conducted experiments with models of varying depths and widths to evaluate their computational complexity. Table 3 presents the final loss values for different model configurations. We observed that changes in model depth and width had minimal impact on the final loss values. This indicates that the DINNs model has relatively low computational complexity, making it suitable for training and prediction on large-scale datasets.

To assess the computing requirements of the DINNs method, we contrasted it with other SEIRV model parameter estimate techniques, including the nonlinear least squares method. Table 4 summarizes the comparison between DINNs and traditional SEIRV parameter estimation methods in terms of training time, memory usage, and inference time. The experimental results demonstrate that although DINNs incur higher training time and memory consumption, they exhibit comparable or superior performance during the inference phase. The traditional model's faster inference time is primarily due to its pre-set parameters, which lack the flexibility to adapt to the dynamic changes of multi-peak epidemics. Conversely, DINNs dynamically estimate parameters, enabling a better fit to the complex epidemic curves observed in real-world scenarios.

Subsequently, we performed a sensitivity analysis on the parameters α, β and γ to assess the robustness of the DINNs model to parameter variations. Figure 7 below illustrates the effect of different parameter changes on the final loss values. We found that variations in these parameters resulted in significant fluctuations in the loss values, indicating that the DINNs model is sensitive to parameter changes. Therefore, precise estimation of these parameters is crucial in practical applications to ensure the accuracy and robustness of the model.

The parameter α represents the decline in immune effect after vaccination and the further transition to exposure, and the parameter γ controls the speed at which infected people recover and develop immunity. The parameter σ represents the rate at which exposed people become infected and further determines the length of the incubation period. A higher value of α signifies a more rapid decline in the vaccine's immunological response, resulting in an increased population of vulnerable individuals, intensifying system instability,

complicating model training, and diminishing forecast accuracy. Conversely, augmenting γ (the recovery rate of infected individuals) and σ (the conversion rate from the incubation period) can diminish transmission risk, streamline the transmission process, expedite the achievement of equilibrium, and enhance the model's capacity to accurately depict the dynamics of infectious diseases, thereby increasing precision. Consequently, augmenting γ and σ while diminishing α can substantially decrease the system's complexity, allowing the DINNs to more precisely represent the disease transmission process aligned with the biological traits of COVID-19.

Discussions and conclusions

During the COVID-19 pandemic, vaccination and control measures became primary methods for combating the spread of the virus, playing a decisive role in understanding the dynamics of the outbreak in China. Thus, quantifying vaccination rates and estimating their impacts remains challenging. Our study introduces a novel approach called the dynamics informed neural network (DINNs), which combines the advantages of ordinary differential equation (ODE) models with deep learning to enhance the predictive capabilities of traditional compartmental models, such as SEIRV. The DINNs framework leverages the universal approximation properties of deep neural networks to estimate time-varying epidemiological parameters. By coupling two subnetworks-one for inferring key parameters like vaccination rates (ϵ) and the other for solving SEIRV differential equations-DINNs can understand the temporal evolution of the epidemic from a data-driven perspective.

Notably, the DINNs algorithm addresses some limitations of traditional dynamical models in simulating COVID-19. For instance, in the SEIR model, vaccination rates and transmission rates are typically set as constants[64,65]. To fit multi-stage epidemic spreads, intervals are often required for infection peaks, which significantly limits the performance of traditional dynamical models. In contrast, our proposed DINNs model effectively resolves this issue by integrating the universal approximation theorem[66] of neural networks with traditional dynamical models, and deriving information on contact rates and vaccination rates from daily new case numbers. In our sensitivity analysis, we observed that variations in neural network depth and width had a minimal impact on the final loss values. This suggests that the DINNs model has relatively low computational complexity, making it suitable for training and prediction on large-scale datasets. However, the predictions of the DINNs model are highly sensitive to initial conditions and parameter estimates. Inaccurate or ambiguous beginning data might disseminate mistakes throughout the model, thereby compromising the trustworthiness of long-term forecasts. The model's success is contingent upon the availability of high-quality, comprehensive data. In reality, data may be missing, delayed, or influenced by reporting biases, which might negatively impact the model's accuracy and robustness. Furthermore, although the DINNs methodology adeptly captures the dynamics of transmission rates and vaccination impacts, it may inadequately consider other influencing factors, such as behavioral modifications, the emergence of novel variants, or regional disparities, unless supplemented with additional data sources or increased model complexity. Subsequent study has to investigate methods to alleviate these constraints, including the incorporation of real-time data assimilation approaches, the enhancement of the model's adaptability to novel variations, and the integration of multi-source data to augment the model's generalizability and robustness. Upon examining the model's sensitivity to parameter variations, we observe that alterations in these parameters significantly affect the loss value. An elevation in α will result in a hastened rate of immune deterioration and heightened system instability; a reduction in γ and σ will precipitate an expedited rate of infection and further complicate the model, demonstrating that the DINNs model is highly responsive to parameter variations, aligning with the biological attributes of actual COVID-19. Consequently, precise estimation of these parameters is essential for maintaining the model's accuracy and resilience in actual applications.

Applying DINNs to COVID-19 data from China demonstrates its exceptional performance in fitting epidemic curves, including cumulative and daily cases, as well as vaccination data. Quantitative evaluation metrics such as MAE, MAPE, MSE, RMSE, and R^2 further validate the high accuracy and stability of DINNs. Additionally, during the early stages of the outbreak, DINNs was able to predict the progression of the epidemic by utilizing daily new case numbers, thus guiding vaccination trends. Integrating deep learning into epidemiological models opens new avenues for data-driven decision-making in public health. Traditional statistical models based on partial differential equations often struggle to adapt to increasingly complex real-world scenarios, such as the emergence of new variants and dynamic control strategies. DINNs harnesses the power of machine learning to accurately describe epidemiological parameters and predict epidemic trajectories, offering a promising solution. Graph neural networks (GNNs) can proficiently represent the intricate interrelations across various geographical regions, allowing DINNs to encapsulate the spatial variability of disease transmission. This integration can enhance forecast accuracy by including aspects such as population movement, alterations in regional policy, and local epidemic dynamics. Utilizing the benefits of GNNs for graph-structured data processing, DINNs models can improve their capacity to depict and forecast the spatiotemporal progression of infectious illnesses, thereby offering more nuanced insights for targeted public health actions. Future research may explore combining DINNs with graph neural networks to account for spatiotemporal factors like population movement.

Data availability

All data used in this study are publicly available and can be accessed from the Johns Hopkins University Center for Systems Science and Engineering (JHU CSSE) and Our World in Data[57,58].

Received: 27 August 2024; Accepted: 2 January 2025
Published online: 15 January 2025

References

1. Calistri, A., Roggero, P. F. & Palù, G. Chaos theory in the understanding of COVID-19 pandemic dynamics. *Gene* 148334 (2024).
2. Hu, S. et al. Races of small molecule clinical trials for the treatment of COVID-19: An up-to-date comprehensive review. *Drug Dev. Res.* **83**, 16–54 (2022).
3. Zhu, N. et al. A novel coronavirus from patients with pneumonia in China, 2019. *N. Engl. J. Med.* **382**, 727–733 (2020).
4. World Health Organization. Who timeline - COVID-19. https://www.who.int/news/item/27-04-2020-who-timeline---COVID-19 (2020). Accessed: 20 Apr 2024.
5. Andrew, R. Preliminary genomic characterisation of an emergent sars-cov-2 lineage in the UK defined by a novel set of spike mutations. *Virological* (2020).
6. Dhar, M. S. et al. Genomic characterization and epidemiology of an emerging sars-cov-2 variant in Delhi, India. *Science* **374**, 995–999 (2021).
7. Tegally, H. et al. Detection of a sars-cov-2 variant of concern in south Africa. *Nature* **592**, 438–443 (2021).
8. Harvey, W. T. et al. Sars-cov-2 variants, spike mutations and immune escape. *Nat. Rev. Microbiol.* **19**, 409–424 (2021).
9. Vespignani, A. et al. Modelling COVID-19. *Nat. Rev. Phys.* **2**, 279–281 (2020).
10. Aziz, M. H. N. et al. Modelling the effect of vaccination program and inter-state travel in the spread of COVID-19 in Malaysia. *Acta. Biotheor.* **71**, 2 (2023).
11. Zhu, Q., Gao, Y., Hu, Q., Hu, D. & Wu, X. A study on the factors influencing the intention to receive booster shots of the COVID-19 vaccine in China based on the information frame effect. *Front. Public Health* **12**, 1258188 (2024).
12. Holmdahl, I. & Buckee, C. Wrong but useful–what COVID-19 epidemiologic models can and cannot tell us. *N. Engl. J. Med.* **383**, 303–305 (2020).
13. Thompson, R. N. et al. Key questions for modelling COVID-19 exit strategies. *Proc. R. Soc. B* **287**, 20201405 (2020).
14. Bretó, C., He, D., Ionides, E. L. & King, A. A. Time series analysis via mechanistic models. *Ann. Appl. Stat.* 319–348 (2009).
15. Kucharski, A. J. et al. Early dynamics of transmission and control of COVID-19: A mathematical modelling study. *Lancet. Infect. Dis.* **20**, 553–558 (2020).
16. Giordano, G. et al. Modelling the COVID-19 epidemic and implementation of population-wide interventions in Italy. *Nat. Med.* **26**, 855–860 (2020).
17. LeCun, Y., Bengio, Y. & Hinton, G. Deep learning. *Nature* **521**, 436–444 (2015).
18. Goodfellow, I., Bengio, Y. & Courville, A. *Deep Learning* (MIT Press, 2016).
19. Jordan, M. I. & Mitchell, T. M. Machine learning: Trends, perspectives, and prospects. *Science* **349**, 255–260 (2015).
20. Esteva, A. et al. Dermatologist-level classification of skin cancer with deep neural networks. *Nature* **542**, 115–118 (2017).
21. Angermueller, C., Pärnamaa, T., Parts, L. & Stegle, O. Deep learning for computational biology. *Mol. Syst. Biol.* **12**, 878 (2016).
22. Aljaaf, A. J., Mohsin, T. M., Al-Jumeily, D. & Alloghani, M. A fusion of data science and feed-forward neural network-based modelling of COVID-19 outbreak forecasting in Iraq. *J. Biomed. Inform.* **118**, 103766 (2021).
23. Alshanbari, H. M. et al. On the implementation of the artificial neural network approach for forecasting different healthcare events. *Diagnostics* **13**, 1310 (2023).
24. Cybenko, G. Approximation by superpositions of a sigmoidal function. *Math. Control Signals Syst.* **2**, 303–314 (1989).
25. Liu, D., Ding, W., Dong, Z. S. & Pedrycz, W. Optimizing deep neural networks to predict the effect of social distancing on COVID-19 spread. *Comput. Ind. Eng.* **166**, 107970 (2022).
26. Kermack, W. O. & McKendrick, A. G. A contribution to the mathematical theory of epidemics. *Proc. R. Soc. Lond. Ser. A Contain. Pap. A Math. Phys. Charact.* **115**, 700–721 (1927).
27. Ferguson, N. M. et al. *Report 9: Impact of Non-pharmaceutical Interventions (NPIs) to Reduce COVID19 Mortality and Healthcare Demand* Vol. 16 (Imperial College London, 2020).
28. Moore, S., Hill, E. M., Tildesley, M. J., Dyson, L. & Keeling, M. J. Vaccination and non-pharmaceutical interventions for COVID-19: A mathematical modelling study. *Lancet. Infect. Dis.* **21**, 793–802 (2021).
29. Kissler, S. M., Tedijanto, C., Goldstein, E., Grad, Y. H. & Lipsitch, M. Projecting the transmission dynamics of sars-cov-2 through the postpandemic period. *Science* **368**, 860–868 (2020).
30. Anderson, R. M. & May, R. M. *Infectious Diseases of Humans: Dynamics and Control* (Oxford University Press, 1991).
31. Hethcote, H. W. The mathematics of infectious diseases. *SIAM Rev.* **42**, 599–653 (2000).
32. Bozzani, F. M. *Incorporating Feasibility in Priority Setting: A Case Study of Tuberculosis Control in South Africa*. Ph.D. thesis, London School of Hygiene & Tropical Medicine (2021).
33. Thompson, J. & Wattam, S. Estimating the impact of interventions against COVID-19: From lockdown to vaccination. *PLoS ONE* **16**, e0261330 (2021).
34. He, M., Tang, S. & Xiao, Y. Combining the dynamic model and deep neural networks to identify the intensity of interventions during COVID-19 pandemic. *PLoS Comput. Biol.* **19**, e1011535 (2023).
35. Samek, W., Montavon, G., Lapuschkin, S., Anders, C. J. & Müller, K.-R. Explaining deep neural networks and beyond: A review of methods and applications. *Proc. IEEE* **109**, 247–278 (2021).
36. Rahmadani, F. & Lee, H. Hybrid deep learning-based epidemic prediction framework of COVID-19: South Korea case. *Appl. Sci.* **10**, 8539 (2020).
37. Dietterich, T. G. Ensemble methods in machine learning. In *International Workshop on Multiple Classifier Systems* 1–15 (Springer, 2000).
38. Tian, Y., Luthra, I. & Zhang, X. Forecasting COVID-19 cases using machine learning models. *MedRxiv* 2020–07 (2020).
39. Ghafouri-Fard, S. et al. Application of machine learning in the prediction of COVID-19 daily new cases: A scoping review. *Heliyon***7** (2021).
40. Ning, X., Jia, L., Wei, Y., Li, X.-A. & Chen, F. Epi-dnns: Epidemiological priors informed deep neural networks for modeling COVID-19 dynamics. *Comput. Biol. Med.* **158**, 106693 (2023).
41. Chimmula, V. K. R. & Zhang, L. Time series forecasting of COVID-19 transmission in Canada using lstm networks. *Chaos Solitons Fractals* **135**, 109864 (2020).
42. Lou, H.-R., Wang, X., Gao, Y. & Zeng, Q. Comparison of Arima model, DNN model and lstm model in predicting disease burden of occupational pneumoconiosis in Tianjin, China. *BMC Public Health* **22**, 2167 (2022).
43. Kong, L. et al. Compartmental structures used in modeling COVID-19: A scoping review. *Infect. Dis. Poverty* **11**, 72 (2022).
44. Cao, L. & Liu, Q. COVID-19 modeling: A review. *ACM Comput. Surv.***57**, https://doi.org/10.1145/3686150 (2024).
45. Ning, X., Guan, J., Li, X.-A., Wei, Y. & Chen, F. Physics-informed neural networks integrating compartmental model for analysing COVID-19 transmission dynamics. *Viruses* **15**, 1749 (2023).
46. Pei, S., Kandula, S., Yang, W. & Shaman, J. Forecasting the spatial transmission of influenza in the united states. *Proc. Natl. Acad. Sci.* **115**, 2752–2757 (2018).
47. Zhao, A. P. et al. Ai for science: Predicting infectious diseases. *J. Saf. Sci. Resilience* (2024).
48. Yeung, A., Roewer-Despres, F., Rosella, L. & Rudzicz, F. Comparison of multiple machine learning-based predictions of growth in COVID-19 confirmed infection cases in countries using non-pharmaceutical interventions and cultural dimensions data: Development and validation (preprint). *J. Med. Intern. Res.*[SPACE]https://doi.org/10.2196/26628 (2020).
49. Annas, S., Pratama, M. I., Rifandi, M., Sanusi, W. & Side, S. Stability analysis and numerical simulation of seir model for pandemic COVID-19 spread in Indonesia. *Chaos Solitons Fractals* **139**, 110072 (2020).

50. Watson, O. J. et al. Global impact of the first year of COVID-19 vaccination: A mathematical modelling study. *Lancet. Infect. Dis.* **22**, 1293–1302 (2022).
51. Schmidhuber, J. Deep learning in neural networks: An overview. *Neural Netw.* **61**, 85–117 (2015).
52. Krizhevsky, A., Sutskever, I. & Hinton, G. E. Imagenet classification with deep convolutional neural networks. *Adv. Neural Inf. Process. Syst.***25** (2012).
53. Hinton, G. et al. Deep neural networks for acoustic modeling in speech recognition: The shared views of four research groups. *IEEE Signal Process. Mag.* **29**, 82–97 (2012).
54. Hornik, K., Stinchcombe, M. & White, H. Multilayer feedforward networks are universal approximators. *Neural Netw.* **2**, 359–366 (1989).
55. Nair, V. & Hinton, G. E. Rectified linear units improve restricted Boltzmann machines. In *Proceedings of the 27th International Conference on Machine Learning (ICML-10)* 807–814 (2010).
56. Kingma, D. P. Adam: A method for stochastic optimization. arXiv preprint arXiv:1412.6980 (2014).
57. Johns Hopkins University Center for Systems Science and Engineering (JHU CSSE). 2019 novel coronavirus COVID-19 (2019-ncov) data repository. https://github.com/CSSEGISandData/COVID-19/tree/master/csse_covid_19_data (2022). Accessed on 16 Oct 2022.
58. Our World in Data. Data on COVID-19 (coronavirus) vaccinations. https://github.com/owid/COVID-19-data/tree/master/public/data/vaccinations (2022).
59. Rousseeuw, P. J. & Hubert, M. Robust statistics for outlier detection. *Wiley Interdiscipl. Rev. Data Min. Knowl. Discov.* **1**, 73–79 (2011).
60. Abadi, M. et al. Tensorflow: Large-scale machine learning on heterogeneous distributed systems. arXiv preprint arXiv:1603.04467 (2016).
61. He, M., Tang, B., Xiao, Y. & Tang, S. Transmission dynamics informed neural network with application to COVID-19 infections. *Comput. Biol. Med.* **165**, 107431 (2023).
62. Colburn, N. How long does it take for the COVID-19 vaccine to work? Wexner Medical Center Blog (2021). Available online.
63. Wu, Y. et al. Incubation period of COVID-19 caused by unique sars-cov-2 strains: A systematic review and meta-analysis. *JAMA Netw. Open* **5**, e2228008 (2022).
64. Chen, Y.-T. Effect of vaccination patterns and vaccination rates on the spread and mortality of the COVID-19 pandemic. *Health Policy Technol.* **12**, 100699 (2023).
65. Salcedo-Varela, G. A., Peñuñuri, F., González-Sánchez, D. & Díaz-Infante, S. Synchronizing lockdown and vaccination policies for COVID-19: An optimal control approach based on piecewise constant strategies. *Opt. Control Appl. Methods* **45**, 523–543 (2024).
66. Voigtlaender, F. The universal approximation theorem for complex-valued neural networks. *Appl. Comput. Harmon. Anal.* **64**, 33–61 (2023).

Author contributions

C.C: Designed the study and wrote the main article, E.A and M.H.N.A: Writing-review and editing. All authors reviewed the manuscript.

Declarations

Competing interests

The authors declare no competing interests.

Additional information

Correspondence and requests for materials should be addressed to M.H.N.A.

Reprints and permissions information is available at www.nature.com/reprints.

Publisher's note Springer Nature remains neutral with regard to jurisdictional claims in published maps and institutional affiliations.